Franck-Condon simulation of the single-vibronic-level emission spectra of HPCl/DPCl and the chemiluminescence spectrum of HPCl, including anharmonicity

Foo-tim Chau,[a] Daniel K. W. Mok, and Edmond P. F. Lee[a),b),c)]
Department of Applied Biology and Chemical Technology, Hong Kong Polytechnic University, Hung Hom, Hong Kong

John M. Dyke
School of Chemistry, University of Southampton, Highfield, Southampton SO17 1BJ, United Kingdom

(Received 29 January 2004; accepted 4 May 2004)

Restricted-spin coupled-cluster single-double plus perturbative triple excitation [RCCSD(T)] potential energy functions (PEFs) were calculated for the $\tilde{X}\,^2A''$ and $\tilde{A}\,^2A'$ states of HPCl employing the augmented correlation-consistent polarized-valence-quadruple-ζ (aug-cc-pVQZ) basis set. Further geometry optimization calculations were carried out on both electronic states of HPCl at the RCCSD(T) level with all electron and quasirelativistic effective core potential basis sets of better than the aug-cc-pVQZ quality, and also including some core electrons, in order to obtain more reliable geometrical parameters and relative electronic energy of the two states. Anharmonic vibrational wave functions of the two states of HPCl and DPCl, and Franck-Condon (FC) factors of the $\tilde{A}\,^2A'$-$\tilde{X}\,^2A''$ transition were computed employing the RCCSD(T)/aug-cc-pVQZ PEFs. Calculated FC factors with allowance for Duschinsky rotation and anharmonicity were used to simulate the single-vibronic-level (SVL) emission spectra of HPCl and DPCl reported by Brandon *et al.* [J. Chem. Phys. **119**, 2037 (2003)] and the chemiluminescence spectrum reported by Bramwell *et al.* [Chem. Phys. Lett. **331**, 483 (2000)]. Comparison between simulated and observed SVL emission spectra gives the experimentally derived equilibrium geometry of the $\tilde{A}\,^2A'$ state of HPCl of $r_e(\mathrm{PCl}) = 2.0035 \pm 0.0015$ Å, $\theta_e = 116.08 \pm 0.60°$, and $r_e(\mathrm{HP}) = 1.4063 \pm 0.0015$ Å via the iterative Franck-Condon analysis procedure. Comparison between simulated and observed chemiluminescence spectra confirms that the vibrational population distribution of the $\tilde{A}\,^2A'$ state of HPCl is non-Boltzmann, as proposed by Baraille *et al.* [Chem. Phys. **289**, 263 (2003)]. © *2004 American Institute of Physics.* [DOI: 10.1063/1.1765654]

I. INTRODUCTION

Recently, we reported *ab initio* calculations on the $\tilde{A}\,^2A'$ and $\tilde{X}\,^2A''$ states, and simulations of the $\tilde{A}\,^2A' \rightarrow \tilde{X}\,^2A''$ emission spectrum, of HPCl employing Franck-Condon (FC) factors computed within the harmonic oscillator model.[1] In this study, our *ab initio* results and spectral simulations confirmed the assignments of the emitter of, and the electronic states involved in, the first observed chemiluminescence spectrum of HPCl reported by Bramwell *et al.*[2] Also some of the vibrational assignments and the T_0 position of the $\tilde{A}\,^2A' \rightarrow \tilde{X}\,^2A''$ transition of Bramwell *et al.* were revised. However, it was noted in Ref. 1 that the experimentally derived equilibrium bond angle θ_e(HPCl) of the $\tilde{A}\,^2A'$ state of HPCl, with a value of 112.6° obtained from the iterative Franck-Condon analysis (IFCA) (see the following section and Ref. 1, and references therein for detail), was significantly smaller than the *ab initio* value of ca. 116.8° obtained at the restricted-spin coupled-cluster single-double plus perturbative triple excitation/correlation-consistent polarized-valence-quadruple ζ [RCCSD(T)/cc-pVQZ] (no g) level of calculation. It was suggested that such a large difference of over 4° between the calculated and experimentally derived IFCA bond angle was possibly due to the inadequacy of the harmonic oscillator model employed in the FC factor calculations. In the present study, effects of including anharmonicity on the simulated emission spectra of HPCl, and, in particular, on the IFCA bond angle of the $\tilde{A}\,^2A'$ state of HPCl, are investigated. In the following sections, we report computed *ab initio* potential energy functions (PEFs) of the $\tilde{A}\,^2A'$ and $\tilde{X}\,^2A''$ states of HPCl, anharmonic vibrational wave functions, FC factors, and spectral simulation of the $\tilde{A}\,^2A' \rightarrow \tilde{X}\,^2A''$ emission of HPCl which include anharmonicity.

During the preparation of the manuscript of the present investigation, a theoretical study[3] on the $\tilde{A}\,^2A' \rightarrow \tilde{X}\,^2A''$ emission of HPCl and HNCl, and a laser induced fluorescence (LIF) and single-vibronic-level (SVL) emission study[4] on HPCl and DPCl have appeared. The former[3] reported B3LYP, CCSD(T), and CASPT2 calculations on the $\tilde{A}\,^2A'$ and $\tilde{X}\,^2A''$ states of HPCl, using the cc-pVTZ basis set, and also FC spectral simulations beyond the harmonic oscillator

[a)]Author to whom correspondence should be addressed. Electronic mail: bcftchau@polyu.edu.hk
[b)]Electronic mail: epl@soton.ac.uk
[c)]Also at University of Southampton.

model, based on a variation-perturbation approach. In general, the *ab initio* results obtained in, and the conclusions drawn from the theoretical investigation of Ref. 3 agree mostly with those of Ref. 1, except that in the comparison between their simulated spectra[3] and the observed chemiluminescence spectrum of Ref. 2, a non-Boltzmann distribution of the populations of the vibrational levels in the upper electronic state of HPCl was proposed. This is in contrast to the conclusion reached in Ref. 1 of a Boltzmann distribution in the low-lying vibrational levels of the upper electronic state with a vibrational temperature of 1000 K. These different conclusions of Refs. 1 and 3 regarding the population distribution of the low-lying vibrational levels of the upper state are also investigated in the present study.

The rotationally resolved LIF and vibrationally resolved SVL emission study of Ref. 4 reported experimentally derived r_0 and estimated r_e^z structures (i.e., the corresponding HP and PCl bond lengths, and the HPCl bond angle) of the $\tilde{A}\,^2A'$ and $\tilde{X}\,^2A''$ states of HPCl, and the fundamental and harmonic vibrational frequencies of these two electronic states of HPCl and DPCl. In addition, CCSD(T)/augmented-coupled-cluster-polarized-valence-triple-ζ aug-cc-pVTZ calculations were carried out on both states of HPCl. One major difference between the chemiluminescence spectrum reported in Ref. 2 and the SVL emission spectra reported in Ref. 4 is that the latter spectra are free from overlapping bands, which arise from emissions from low-lying vibrational levels of the upper electronic state, as observed in the chemiluminescence spectrum. In this connection, the simpler SVL emission spectra will be considered first in the section dealing with the comparison between the simulated and observed spectra, before the chemiluminescene spectrum is discussed.

II. THEORETICAL CONSIDERATIONS AND COMPUTATIONAL DETAILS

A. *Ab initio* calculations, potential energy functions, and Franck-Condon factor calculations

Restricted-spin coupled-cluster single-double[5] plus perturbative triple[6] excitation [RCCSD(T)] calculations were carried out on the $\tilde{A}\,^2A'$ and $\tilde{X}\,^2A''$ states of HPCl, employing the aug-cc-pVQZ basis set.[7] The $1s^22s^22p^6$ core electrons of P and Cl were frozen in these RCCSD(T) calculations. 171 RCCSD(T)/aug-cc-pVQZ energy points were scanned on the electronic energy surface of the $\tilde{X}\,^2A''$ state of HPCl in the geometrical ranges of $1.21<r(\mathrm{HP})<1.77$ Å, $1.84<r(\mathrm{PCl})<2.40$ Å, and $55.0<\theta(\mathrm{HPCl})<135.0°$, and 163 energy points were scanned on the $\tilde{A}\,^2A'$ surface in the geometrical ranges of $1.198<r(\mathrm{HP})<1.758$ Å, $1.810<r(\mathrm{PCl})<2.370$ Å, and $84.0<\theta(\mathrm{HPCl})<148.0°$. Polynomial functions of the following form were fitted to the corresponding computed *ab initio* total energies to give the potential energy functions (PEFs) of the $\tilde{X}\,^2A''$ and $\tilde{A}\,^2A'$ states of HPCl.

$$\mathbf{V}=\sum_{ijk} C_{ijk}(S_1)^i(S_2)^j(S_3)^k+V_{\mathrm{eqm}}. \quad (1)$$

The bending coordinate suggested by Carter and Handy,[8]

$$S_2=\Delta\theta+\alpha\Delta\theta^2+\beta\Delta\theta^3,$$

has been employed for S_2, where $\Delta\theta$ is the displacement of the bond angle from the equilibrium value, $(\theta-\theta_e)$, while S_1 and S_3 are the displacements of the HP and PCl bond lengths from the equilibrium values, $(r-r_e)$, respectively.

The fitting of the PEFs, the variational calculations of the anharmonic vibrational wave functions and the FC factor calculations were carried out as described previously.[9,10] In brief, Watson's Hamiltonian[11,12] for a nonlinear molecule was used, and both anharmonicity and Duschinsky rotation were included in the FC factor calculations. Here, only some technical details specific to the present study are given and these are as follows: Anharmonic vibrational wave functions were expressed as linear combinations of harmonic oscillator functions, $h(v_1,v_2,v_3)$, where v_1, v_2, and v_3 denote the quantum numbers of the harmonic basis functions for the HP stretching, bending, and PCl stretching modes, respectively. Harmonic basis functions with vibrational quantum numbers of up to $h(6,20,10)$ and a restriction of $v_1+v_2+v_3<20$ were included in the variational calculations of the $\tilde{X}\,^2A''$ state. For the $\tilde{A}\,^1A'$ state, harmonic basis functions of up to $h(6,10,10)$, with a restriction of $v_1+v_2+v_3<10$ were considered.

The IFCA procedure was carried out (see Refs. 9 and 10 for details) with the geometry of the $\tilde{X}\,^2A''$ state fixed to the experimentally derived, estimated equilibrium (r_e^z) geometry of Ref. 4, while the geometrical parameters of the $\tilde{A}\,^2A'$ state were varied systematically, until the best match between simulated and observed SVL emission spectra was obtained (see also the following section for a more detailed description, which includes the *ab initio* calculations). Vibronic components in the SVL $\tilde{A}\,^2A'\rightarrow\tilde{X}\,^2A''$ emission spectra of HPCl/DPCl were simulated using Gaussian functions with a full width at half maximum (FWHM) of 15 cm^{-1}, which is a spectral resolution slightly better than that of the observed SVL emission spectra of Ref. 4. For simulated chemiluminescence spectra, a FWHM of 1 nm ($\sim$30 cm^{-1} in the visible region of 400–600 nm) was used (cf. an experimental resolution of 0.32 nm quoted in Ref. 2 for the wavelength region of 400–600 nm). The relative intensity of each vibrational component in a simulated spectrum is given by the product of the corresponding computed anharmonic FC factor and a frequency factor of power 4.

B. Further geometry optimization calculations

In order to obtain more reliable computed equilibrium geometrical parameters of the $\tilde{A}\,^2A'$ and $\tilde{X}\,^2A''$ states of HPCl, and transition energies (T_e and T_0) between the two states, further geometry optimization calculations employing basis sets of better quality than the aug-cc-pVQZ basis set were carried out at the RCCSD(T) level of theory. First, the aug-cc-p($d+$Q)Z basis sets,[13] which contain an extra tight d function added to the original aug-cc-pVQZ basis sets for the second row elements, were used for P and Cl. This is because tight d polarization functions have been found to be impor-

tant in the basis set at the Hartree-Fock level of theory for second row elements (see Refs. 13 and 14, and references therein).

Second, in addition to the valence electrons, the $2s^2 2p^6$ core electrons of P and Cl were correlated in the RCCSD(T) calculations (i.e., only the $1s^2$ electrons of P and Cl are frozen) and the energy-weighed core-valence aug-cc-pwCVQZ basis sets[15] were used for P and Cl. This is to investigate the effects of core-core and core-valence correlation on the minimum-energy geometries of the two states of HPCl, which contains the second row elements, P and Cl (see, for examples, Ref. 14, and references therein). It should be noted that these calculations including the core electrons were extremely, computationally demanding (in terms of both memory and CPU time).

Third, the cc-pV5Z basis set was employed to examine the effects of better valence description than the valence QZ quality. The augmented (or diffuse) part of the aug-cc-pV5Z basis set has been excluded, because its inclusion would lead to unmanageably demanding calculations. Nevertheless, basis sets, which make use of effective core potentials (ECPs) to account for core electrons, and are of the augmented polarized valence 5Z quality, were considered for P and Cl. The following contracted $[6s6p5d4f3g2h]$ valence basis sets of the aug-cc-pV5Z quality, which coupled with the respective quasirelativistic energy-consistent pseudopotentials (ECP10MWB) of the Stuttgart/Koeln group,[16] were designed to describe the valence $3s$ and $3p$ shells of the P and Cl atoms.

(a) P: 15 even-tempered *s* primitives (ratio=1.75; center exponent=1.5) and 13 even-tempered *p* primitives (1.75; 0.8) were contracted to $[1s1p]$, with the contraction coefficients obtained from a restricted open shell Hartree Fock (ROHF) calculation of the neutral atom employing the $15s13p$ primitives uncontracted, plus the following uncontracted functions: $5s$(2.5; 0.25), $5p$(2.4; 0.18), $5d$(2.5; 2.0), $4f$ (exponents; 0.768 32, 0.2744, 0.098, 0.035), $3g$(0.49, 0.14, 0.04), and $2h$(0.24, 0.06).

(b) Cl: 15 even-tempered *s* primitives (ratio=1.8; center exponent=2.0) and 13 even-tempered *p* primitives (1.75; 0.8) were contracted to $[1s1p]$, with the contraction coefficients obtained from an ROHF calculation of the neutral atom employing the $15s13p$ primitives uncontracted, plus the following uncontracted functions: $5s$(2.5; 0.45), $5p$(2.6; 0.3), $5d$(2.6; 0.3), $4f$ (exponents; 1.8, 0.6, 0.2, 0.066 667), $3g$(1.75, 0.388 89, 0.086 419 7), and $2h$(0.35, 0.077 778).

The above ECP10MWB $[6s6p5d4f3g2h]$ basis sets for P and Cl (ECP-AV5Z in short) were used together with the aug-cc-pV5Z basis set for H. Calculations using these 5Z quality basis sets of cc-pV5Z and ECP-AV5Z explore the effects of basis set extension towards the complete basis set (CBS) limit on the minimum-energy geometries of the two states of HPCl and their relative electronic energies. In addition, the quasirelativistic ECPs employed for P and Cl in the ECP-AV5Z basis sets described above also account for a certain amount of relativistic contribution. Summing up, various effects, arising from basis size extension towards the CBS limit, electron correlation of core electrons, and relativistic contributions of the second row elements, P and Cl, on the computed equilibrium geometrical parameters of, and transition energies between, the $\tilde{A}\,^2A'$ and $\tilde{X}\,^2A''$ states of HPCl were investigated by carrying out RCCSD(T) geometry optimization calculations employing various basis sets described above.

All the RCCSD(T) calculations carried out in the present study were performed using the MOLPRO suite of programs.[17]

TABLE I. The RCCSD(T)/aug-cc-pVQZ PEFs of the $\tilde{X}\,^2A''$ and $\tilde{A}\,^2A'$ states of HPCl [see text and Eq. (1)].

$C(I,j,k)$	$\tilde{X}\,^2A''$	$\tilde{A}\,^2A'$
002	0.3269	0.3652
200	0.3785	0.3768
020	0.1051	0.0561
101	0.0038	−0.0125
011	0.0558	0.0162
110	−0.0120	0.0086
003	−0.5186	−0.6241
300	−0.6485	−0.7243
030	−0.0307	0.0016
102	−0.0225	−0.0230
012	−0.0937	−0.0347
201	0.0272	0.0037
210	−0.0016	0.0147
021	−0.1286	−0.0537
120	−0.0187	−0.0410
111	−0.0201	−0.0220
004	0.4136	0.4795
400	0.5343	0.5914
040	0.0074	−0.0129
103	0.0352	0.0356
013	0.0505	0.0060
301	0.0025	0.0068
310	0.0136	−0.0351
031	0.0672	0.0194
130	−0.0097	0.0252
202	−0.0343	−0.0726
022	0.0645	0.0030
220	−0.0380	−0.0358
112	0.0555	0.0077
211	−0.0214	−0.0117
121	0.0176	0.0160
R_e(P-Cl)/Å	2.0511	2.0142
R_e(H-P)/Å	1.4209	1.4101
$\angle(\mathrm{HPCl})_e$/°	95.1664	116.9346
rms/hartree (cm^{-1})	4.7×10^{-5}(10.3)	6.4×10^{-5}(14.0)

III. RESULTS AND DISCUSSION

The RCCSD(T)/aug-cc-pVQZ PEFs of the $\tilde{X}\,^2A''$ and $\tilde{A}\,^2A'$ states of HPCl, and some of the computed anharmonic vibrational energies and wave functions of the two states are given in Tables I and II respectively. The calculated equilibrium geometrical parameters, harmonic and fundamental vibrational frequencies of, and transition energies (T_0/T_e) between, the $\tilde{X}\,^2A''$ and $\tilde{A}\,^2A'$ states of HPCl (DPCl) are summarized in Tables III to VI, together with previously calculated and experimentally measured/derived values for comparison. Simulated spectra are shown in Figs. 1–6 together with the corresponding experimental spectra for comparison.

TABLE II. Calculated energies E_{vib} (cm^{-1}) and anharmonic vibrational wave functions Ψ_{vib} in terms of harmonic basis functions (see text) of some low-lying vibrational levels of the $\tilde{X}\,^2A''$ and $\tilde{A}\,^2A'$ states of HPCl.

E_{vib}	Ψ_{vib} of the $\tilde{X}\,^2A''$ state
0.000	$0.9932h(0,0,0)-0.0808h(1,0,0)+0.0642h(0,0,1)$ $-0.0299h(3,0,0)+0.0293h(0,1,0)$
528.659	$-0.9793h(0,0,1)-0.1613h(0,0,2)+0.0790h(1,0,1)$ $+0.0644h(0,0,0)-0.0307h(0,1,1)$
877.123	$-0.9898h(0,1,0)-0.1006h(0,1,1)-0.0699h(0,2,0)$ $-0.0334h(1,3,0)+0.0300h(1,1,0)$
1051.932	$0.9388h(0,0,2)+0.2767h(0,0,3)-0.1625h(0,0,1)$ $-0.0750h(1,0,2)+0.0534h(0,0,4)$
1401.246	$0.9651h(0,1,1)+0.2106h(0,1,2)-0.1011h(0,1,0)$ $+0.0702h(0,2,1)+0.0360h(0,1,3)$
1570.048	$0.8581h(0,0,3)+0.3945h(0,0,4)-0.2804h(0,0,2)$ $+0.1033h(0,0,5)+0.0803h(0,0,6)$
1746.993	$0.9664h(0,2,0)+0.1458h(1,0,0)+0.1336h(0,2,1)$ $+0.1173h(0,3,0)-0.0709h(0,1,0)$
1919.965	$-0.9065h(0,1,2)-0.3304h(0,1,3)+0.2131h(0,1,1)$ $-0.0783h(0,1,4)-0.0677h(0,2,2)$
2083.455	$-0.7282h(0,0,4)-0.4967h(0,0,5)+0.4029h(0,0,3)$ $-0.1686h(0,0,6)-0.1171h(0,0,7)$
2265.935	$-0.9036h(0,2,1)-0.2448h(0,2,2)+0.2446h(1,0,0)$ $-0.1239h(1,0,1)-0.1114h(0,3,1)$
2278.549	$-0.9122h(1,0,0)+0.2450h(2,0,0)-0.2167h(0,2,1)$ $+0.1744h(0,2,0)-0.0821h(1,0,1)$
2433.532	$0.8020h(0,1,3)+0.4434h(0,1,4)-0.3369h(0,1,2)$ $+0.1381h(0,1,5)+0.0920h(0,1,6)$
2594.024	$0.5651h(0,0,6)+0.5514h(0,0,5)-0.5119h(0,0,4)$ $+0.2394h(0,0,7)+0.1566h(0,0,8)$
2609.757	$-0.9214h(0,3,0)-0.2477h(1,1,0)-0.1665h(0,4,0)$ $-0.1610h(0,3,1)+0.1231h(0,2,0)$
E_{vib}	Ψ_{vib} of the $\tilde{A}\,^2A'$ state
0.000	$0.9921h(0,0,0)+0.0819h(1,0,0)+0.0697h(0,0,1)$ $+0.0345h(3,0,0)-0.0335h(1,2,0)$
558.616	$-0.9759h(0,0,1)-0.1713h(0,0,2)-0.0800h(1,0,1)$ $+0.0701h(0,0,0)-0.0340h(3,0,1)$
641.242	$-0.9902h(0,1,0)-0.0911h(0,1,1)+0.0574h(0,2,0)$ $+0.0571h(1,3,0)-0.0310h(3,1,0)$
1110.287	$0.9302h(0,0,2)+0.2908h(0,0,3)-0.1737h(0,0,1)$ $+0.0756h(1,0,2)+0.0623h(0,0,4)$
1196.615	$0.9669h(0,1,1)+0.2000h(0,1,2)-0.0922h(0,1,0)$ $-0.0667h(0,2,1)-0.0562h(1,3,1)$
1270.096	$0.9702h(0,2,0)-0.1217h(1,0,0)+0.1098h(0,2,1)$ $-0.0926h(0,3,0)-0.0781h(1,4,0)$
1655.136	$-0.8397h(0,0,3)-0.4103h(0,0,4)+0.2975h(0,0,2)$ $-0.1181h(0,0,5)-0.0887h(0,0,6)$
1745.006	$0.9092h(0,1,2)+0.3212h(0,1,3)-0.2045h(0,1,1)$ $+0.0773h(0,1,4)-0.0741h(0,2,2)$
1822.059	$-0.9382h(0,2,1)-0.2224h(0,2,2)+0.1179h(1,0,1)$ $+0.1149h(0,2,0)+0.1046h(0,3,1)$
1885.977	$0.9305h(0,3,0)-0.2033h(1,1,0)-0.1392h(1,3,0)$ $-0.1308h(0,4,0)+0.1229h(0,3,1)$

A. The *ab initio* potential energy functions and the anharmonic vibrational wave functions of the $\tilde{A}\,^2A'$ and $\tilde{X}\,^2A''$ states of HPCl

The RCCSD(T)/aug-cc-pVQZ PEFs of the $\tilde{A}\,^2A'$ and $\tilde{X}\,^2A''$ states of HPCl are given in Table I. The root mean square (rms) deviations of the fitted potentials from the computed single point energies are 14.0 and 10.3 cm^{-1} for the $\tilde{A}\,^2A'$ and $\tilde{X}\,^2A''$ states, respectively.

Table II shows the computed energies and anharmonic wave functions of some low-lying vibrational levels of the $\tilde{A}\,^2A'$ and $\tilde{X}\,^2A''$ states of HPCl expressed as linear combinations of harmonic basis functions (five largest harmonic terms are shown). First, based on the computed anharmonic wave functions, the normal modes correspond largely to the HP stretching, bending, and PCl stretching modes, respectively, and the vibrational designations of the anharmonic vibrational wave functions follow closely with those of the leading harmonic basis functions at least for most of the low-lying vibrational levels shown in Table II. Second, other than the HP stretching mode, which is expected to be strongly anharmonic, the PCl stretching mode is also significantly anharmonic in both the $\tilde{A}\,^2A'$ and $\tilde{X}\,^2A''$ states of HPCl. This anharmonic effect in the PCl stretching mode is reflected in the calculated anharmonic vibrational wave functions with leading harmonic basis functions of $h(0,0,v_3)$, where $v_3 \geqslant 3$. It can be seen that, for these higher vibrational levels of the PCl stretching mode, the coefficients of the leading harmonic terms become significantly smaller than unity as v_3 increases, and contributions from other harmonic terms become significant. Nevertheless, these computed anharmonic wave functions suggest a purely PCl stretching mode with negligibly small coupling with the bending and/or HP stretching modes. Third, anharmonic effects are also found to be significant in combination levels involving the PCl stretch. For example, the anharmonic wave function of the $\tilde{X}\,^2A''$ state with $h(0,1,3)$ as its leading harmonic term has significant contribution also from $h(0,1,4)$ (with a calculated coefficient of 0.44; see Table II). Fourth, anharmonic vibrational wave functions of very close calculated energies show some "mode mixing," as expected. For example, for the vibrational levels of the $\tilde{X}\,^2A''$ state with $h(1,0,0)$ and $h(0,2,1)$ as the leading harmonic terms in their anharmonic wave functions, which are calculated to be only 12.6 cm^{-1} apart in energy, the anharmonic wave functions show significant mixing (see Table II). Finally, in general, the computed anharmonic vibrational wave functions for both states of DPCl behave in similar ways as those of HPCl discussed, though the magnitudes of anharmonic effect and mode mixing in DPCl are slightly smaller than in HPCl.

B. The equilibrium geometrical parameters of the $\tilde{A}\,^2A'$ and $\tilde{X}\,^2A''$ states of HPCl

Calculated minimum-energy geometrical parameters of the two states of HPCl and the corresponding experimentally derived values are summarized in Table III. We have only included previous *ab initio* results of relatively higher levels in Table III (for earlier and lower level results from *ab initio* and/or density functional calculations, see Refs. 3 and 4, and references therein). When the levels of theory employed to obtain the calculated values as shown in Table III are considered, it is clear that the levels used in the present study are superior to those reported previously. Therefore, we will focus on the results obtained in the present study from here onward. For the $\tilde{X}\,^2A''$ state of HPCl, the ranges of the calculated r_e(HP), θ_e(HPCl), and r_e(PCl) values at the RCCSD(T) level with basis sets of, or better than, the aug-cc-pVQZ quality are between 1.4166 and 1.4213, 94.97 and

TABLE III. The computed and experimentally derived geometrical parameters [Equilibrium geometrical parameters, unless otherwise stated; estimated uncertainties/errors given in parentheses (see original works for details); for earlier works see Refs. 1, 3, and 4, and references therein.] of the $\tilde{X}\,^2A''$ and $\tilde{A}\,^2A'$ states of HPCl.

$\tilde{X}\,^2A''$	R_e(HP)/Å	θ_e(HPCl)/°	R_e(PCl)/Å	Reference
RCCSD(T)/aug-cc-pVQZ(PEF)	1.4209	95.17	2.0511	Present
RCCSD(T)/aug-cc-pVQZ[a]	1.4213	95.11	2.0517	Present
RCCSD(T)/aug-cc-pV(d+Q)Z[a]	1.4200	95.23	2.0462	Present
RCCSD(T)/aug-cc-pwCVQZ[a]	1.4166	95.22	2.0397	Present
RCCSD(T)/cc-pV5Z[a]	1.4195	95.22	2.0437	Present
RCCSD(T)/ECP-AV5Z[a]	1.4192	94.97	2.0478	Present
Averaged	1.4196(30)	95.15(18)	2.0467(70)	Present
CCSD(T)/aug-cc-pVTZ	1.425	94.9	2.067	4
CCSD(T)/cc-pVTZ	1.4239	95.18	2.0633	3
CASPT2/cc-pVTZ	1.4250	94.64	2.0628	3
RCCSD(T)/cc-pVQZ (no g)	1.4188	95.06	2.0570	1
r_0	1.4331(36)	95.0(4)	2.0418(6)	4
r_z	1.4279(23)	95.02(27)	2.0433(4)	4
r_e^z	1.4158(23)	95.02(27)	2.0388(23)	4
$\tilde{A}\,^2A'$				
RCCSD(T)/aug-cc-pVQZ(PEF)	1.4102	116.93	2.0142	Present
RCCSD(T)/aug-cc-pVQZ[a]	1.4113	116.72	2.0150	Present
RCCSD(T)/aug-cc-pV(d+Q)Z[a]	1.4100	116.76	2.0094	Present
RCCSD(T)/aug-cc-pwCVQZ[a]	1.4072	116.70	2.0029	Present
RCCSD(T)/cc-pV5Z[a]	1.4095	116.73	2.0074	Present
RCCSD(T)/ECP-AV5Z[a]	1.4093	116.71	2.0104	Present
Averaged	1.4096(24)	116.76(17)	2.0099(70)	Present
Ab initio changes[b]	1.4058	116.63	2.0020	Present
CCSD(T)/aug-cc-pVTZ	1.414	116.6	2.030	4
CCSD(T)/cc-pVTZ	1.4124	116.54	2.0294	3
CASPT2/cc-pVTZ	1.4111	116.96	2.0246	3
RCCSD(T)/cc-pVQZ (no g)	1.4080	116.76	2.0205	1
r_0	1.4231(38)	115.4(2)	2.0078(4)	4
r_z	1.4168(20)	115.53(12)	2.0093(2)	4
r_e^z	1.4067(20)	115.53(12)	2.0050(2)	4
IFCA (harmonic)		112.6	2.013	1
IFCA (anharmonic)[c]	1.4063(15)	116.08(60)	2.0035(15)	Present

[a]Optimized geometry; see text.

[b]Experimental r_e^z values of the $\tilde{X}\,^2A''$ state of HPCl plus the averaged *ab initio* geometrical changes upon deexcitation; see text.

[c]See text.

95.23°, and 2.0397 and 2.0517 Å, respectively. The very narrow spreads of the computed geometrical parameters of 0.0047, 0.26° and 0.0120 Å, respectively, suggest a high degree of consistency in these theoretical values. Therefore, it is concluded that these *ab initio* results should be reasonably reliable and any further improvements in the level of calculation would not lead to any significant changes of the optimized geometrical parameters of the $\tilde{X}\,^2A''$ state of HPCl. The averaged calculated values of r_e(HP), θ_e(HPCl), and r_e(PCl) are 1.4196±0.0030, 95.15±0.18°, and 2.0467 ±0.0070 Å, which agree with the experimentally derived, estimated r_e^z values of Ref. 4 to within the combined theoretical and experimental uncertainties.

Comparing the calculated and experimentally derived equilibrium geometrical parameters of the $\tilde{X}\,^2A''$ state of HPCl in more detail, the computed equilibrium bond lengths obtained using the aug-cc-pwCVQZ basis set [correlating the core $2s^62p^6$ electrons of P and Cl explicitly in the RCCSD(T) calculations] agree best with the experimentally derived r_e^z values[4] (to within 0.001 Å). For the bond angle, the RCCSD(T)/ECP-AV5Z, value agrees best with the r_e^z value (to within 0.05°). If the computed equilibrium geometrical parameters, obtained using basis sets of better than the aug-cc-pVQZ quality (i.e., the aug-cc-pwCVQZ, cc-pV5Z, and ECP-AV5Z basis sets) are considered, the averaged calculated values of r_e(HP), θ_e(HPCl), and r_e(PCl) are 1.4184±0.0018, 95.14±0.17°, and 2.0437±0.0041 Å, respectively. These values agree with the corresponding experimentally derived, estimated r_e^z values of Ref. 4 to within 0.0026 Å, 0.12°, and 0.0049 Å. Such good agreement between theory and experiment confirms the reliability of these equilibrium geometrical parameters of the $\tilde{X}\,^2A''$ state of HPCl.

For the $\tilde{A}\,^2A'$ state of HPCl, the spreads of the calculated r_e(HP), θ_e(HPCl), and r_e(PCl) values at the RCCSD(T) level with basis sets of, or better than, the aug-cc-pVQZ quality are 0.0041, 0.23°, and 0.0076 Å, respectively (Table III), which are even smaller than those of the $\tilde{X}\,^2A''$ state, indicating that these *ab initio* geometrical parameters are highly consistent and hence should be reasonably reliable. The averaged calculated r_e(HP), θ_e(HPCl),

TABLE IV. Computed and observed harmonic and fundamental vibrational frequencies [The harmonic and fundamental vibrational frequencies of the PH stretching, bending, and PCl stretching modes, respectively (quoted uncertainties are in parentheses; see original works).] (cm^{-1}) of the $\tilde{X}\,^2A''$ state of HPCl and DPCl.

HPCl $\tilde{X}\,A''$	ω_1	ω_2	ω_3	v_1	v_2	v_3	Ref.
RCCSD(T)/aug-cc-pVQZ	2395.3	894.7	536.3	2278.5	877.0	528.7	Present
CCSD(T)/aug-cc-pVTZ	2368	882	523				4
CCSD(T)/cc-pVTZ	2369	885	559	2298	879	523	3
CASPT2/cc-pVTZ	2446	906	533	2400	900	526	3
QCISD/6-311G($3df$,$3pd$)	2403.7	907.8	510.7				1
CASSCF/6-311G($2df$,$2pd$)	2281	893	505				2
Chemiluminescence		868(2)	529(8)		888	531	2
SVL emission[a]	2277.9(12)	883.19(36)	531.25(95)	2277.3	879.2	529.9	4
DSiF $\tilde{X}\,^2A''$							
RCCSD(T)/aug-cc-pVQZ	1716.3	647.5	535.7	1655.7	638.1	528.6	Present
CCSD(T)/aug-cc-pVTZ	1688	639	486				4
SVL emission[a]	1656.69(59)	641.39(18)	530.90(45)	1656.8	640.7	529.3	4

[a]An estimated accuracy of ± 3 cm^{-1} was given for the monochromater scan; see Ref. 4 for detail.

and r_e(PCl) values are 1.4096 ± 0.0024, $116.76 \pm 0.17°$, and 2.0099 ± 0.0070 Å, respectively. The discrepancies between the averaged calculated bond lengths of the $\tilde{A}\,^2A'$ state of HPCl and the experimentally derived, estimated r_e^z values of Ref. 4 are less than 0.0049 Å, which is within the combined uncertainties associated with the theoretical and experimental values. However, for the bond angle of the $\tilde{A}\,^2A'$ state of HPCl, the r_e^z value from Ref. 4 is smaller than all the calculated values shown in Table III by over 1°. It should be noted that the *ab initio* bond angles of the $\tilde{A}\,^2A'$ state of HPCl are extremely consistent at all levels of calculation, and the optimized bond angles from calculations with the larger basis sets of aug-cc-pwCVQZ, cc-pV5Z, and ECP-AV5Z converge to a value of $116.71 \pm 0.02°$. It is unlikely that the theoretical value of the bond angle of the $\tilde{A}\,^2A$ state of HPCl would change significantly with any further improvement in the level of calculation.

Considering the changes of the equilibrium geometrical parameters upon deexcitation from the $\tilde{A}\,^2A'$ state to the $\tilde{X}\,^2A''$ state, the experimentally derived, estimated r_e^z values

TABLE V. Computed and observed harmonic and fundamental vibrational frequencies [The harmonic and fundamental vibrational frequencies of the PH stretching, bending, and PCl stretching modes, respectively (quoted uncertainties are in parentheses; see original works).] (cm^{-1}) of the $\tilde{A}\,^2A'$ state of HPCl and DPCl.

HPCl $\tilde{A}\,^2A'$	ω_1	ω_2	ω_3	v_1	v_2	v_3	Reference
RCCSD(T)/aug-cc-pVQZ	2386.6	667.6	568.8	2221.5	641.2	558.6	Present
CCSD(T)/aug-cc-pVTZ	2303	634	503				4
CCSD(T)/cc-pVTZ	2370	656	554	2260	645	546	3
CASPT2/cc-pVTZ	2375	676	544	2265	664	537	3
QCISD/6-311G($3df$,$3pd$)	2407.1	669.8	563.7				1
CASSCF/6-311G($2df$,$2pd$)	2236	672	524				2
Chemiluminescence		622(4)			633		2
LIF[a]	2214.9(10)	639.68(59)	554.98(93)	2214.9	631.4	555.0	4
DPCl $\tilde{A}\,^2A'$							
RCCSD(T)/aug-cc-pVQZ	1713.4	480.8	574.4	1625.5	467.5	564.3	Present
CCSD(T)/aug-cc-pVTZ	1740	483	596				4
LIF[a]	1621.54(61)	462.74(20)	563.61(37)	[1621.5][b]	459.4	560.7	4

[a]The estimated accuracy of low-resolution LIF experiments from calibrated spectra is 0.5 cm^{-1}; see Ref. 4 for detail.

[b]The $\tilde{A}(1,0,0) \leftarrow \tilde{X}(0,0,0)$ LIF band of DPCl was too weak to assign. The separation between the observed $\tilde{A}(1,1,0)$ and (0,1,0) LIF bands is 1609.50 cm^{-1}. The ν_1' value of DPCl used as observed input data for normal coordinate analysis and force field refinement is given in squared brackets in the table. See Ref. 4 for detail.

TABLE VI. Calculated and observed values of T_e and T_0 of the $\tilde{A}\,^2A'$-$\tilde{X}\,^2A''$ transition of HPCl/DPCl.

HPCl	T_0[a]/eV (cm^{-1})	T_e[b]/eV (cm^{-1})	Reference
RCCSD(T)/aug-cc-pVQZ	2.725 (21 978.9)	2.738 (22 080.5)	Present
RCCSD(T)/aug-cc-p(d+Q)Z	2.721 (21 948.6)	2.734 (22 050.3)	Present
RCCSD(T)/aug-cc-pwCVQZ	2.731 (22 030.4)	2.744 (22 132.0)	Present
RCCSD(T)/cc-pV5Z	2.724 (21 974.3)	2.737 (22 075.9)	Present
RCCSD(T)/ECP-AV5Z	2.752 (22 195.5)	2.765 (22 297.1)	Present
Averaged	2.731 (22 025.5)	2.743 (22 127.2)	Present
RCCSD(T)/cc-pV5Z (no h)[c]	2.727 (21 993.3)	2.740 (22 095.9)	1
CCSD(T)/cc-pVTZ	2.76 (22 261)	2.772 (22 354.4)	3
CASPT2/cc-pVTZ	2.78 (22 422)	2.799 (22 578.7)	3
CCSD(T)/aug-cc-pVTZ	2.738 (22 082)		4
Chemiluminescence[d]	2.71 (21 844)		2
LIF	2.714 (21 891.3207)	2.732 (22 032.71)	4
LIF		2.727 (21 992.97)[e]	
DHCl			
RCCSD(T)/aug-cc-pVQZ	2.730 (22 015.1)	2.738 (22 080.5)	Present
RCCSD(T)/aug-cc-p(d+Q)Z	2.726 (21 984.8)	2.734 (22 050.3)	Present
RCCSD(T)/aug-cc-pwCVQZ	2.736 (22 066.6)	2.744 (22 132.0)	Present
RCCSD(T)/cc-pV5Z	2.729 (22 010.5)	2.737 (22 075.9)	Present
RCCSD(T)/ECP-AV5Z	2.756 (22 231.7)	2.765 (22 297.1)	Present
Averaged	2.735 (22 061.7)	2.743 (22 127.2)	Present
LIF	2.720 (21 935.5880)	2.731 (22 026.14)	4
LIF		2.728 (22 001.04)[e]	

[a]Zero-point vibrational energy (ZPVE) corrections for calculated T_0 values of the present study have employed the RCCSD(T)/aug-cc-pVQZ harmonic frequencies obtained from the PEFs.

[b]Experimental T_e values were obtained by correcting ZPVEs employing the experimentally derived harmonic vibrational frequencies of Ref. 4; see also footnote e.

[c]Using the optimized geometries and harmonic vibrational frequencies obtained at the QCISD/6-311G($3df$,$3pd$) level of calculation. See Ref. 1 for detail.

[d]The original T_0 position in Ref. 2 is assigned to 2.64 eV (21 305 cm^{-1}). The value given in the table is the revised value from Ref. 1; see Ref. 1 for detail.

[e]ZPVE correction employing the RCCSD(T)/aug-cc-pVQZ harmonic vibrational frequencies obtained from the PEFs.

from Ref. 4 give changes of +0.0091, −20.51°, and +0.0338 Å in r_e(HP), θ_e(HPCl), and r_e(PCl), respectively. The corresponding geometrical changes from the RCCSD(T)/aug-cc-pVQZ PEFs are +0.0107, −21.76°, and +0.0369 Å and those from the averaged calculated values are +0.0100, −21.61°, and +0.0368 Å. The agreement between the theoretically and experimentally derived geometrical changes upon deexcitation in the bond lengths of within 0.0031 Å is excellent, particularly with the averaged calculated equilibrium geometrical parameters. However, the discrepancy between the *ab initio* and experimentally derived, estimated r_e^z change of the equilibrium bond angles upon deexcitation of over 1° casts doubt on the quoted uncertainties of 0.27° and 0.12° associated with the experimentally derived, estimated r_e^z bond angle of the $\tilde{X}\,^2A''$ and $\tilde{A}\,^2A'$ states of HPCl, respectively, given in Ref. 4. The comparison between theoretically and experimentally obtained geometrical parameters, particularly the bond angle of the $\tilde{A}\,^2A'$ state of HPCl, will be further discussed, when the simulated and observed SVL emission spectra are compared.

C. Harmonic and fundamental vibrational frequencies of the $\tilde{X}\,^2A''$ and $\tilde{A}\,^2A'$ states of HPCl and DPCl

From Table IV, the agreement between the RCCSD(T)/aug-cc-pVQZ fundamental vibrational frequencies of the $\tilde{X}\,^2A''$ state of HPCl and DPCl obtained from the PEF of the present study and the observed values from the SVL emission spectra of Ref. 4 is excellent for all three vibrational modes. The small differences between theory and experiment of less than 3 cm^{-1} suggest that the *ab initio* PEF reported here for the $\tilde{X}\,^2A''$ state of HPCl is highly accurate. The agreement between the computed fundamental vibrational frequencies obtained at lower levels of calculation from Ref. 3 and the observed values of Ref. 4 is generally not as good, as expected, and hence we focus on the higher level results of the present study from here onward. Regarding the harmonic vibrational frequencies of the $\tilde{X}\,^2A''$ state of HPCl and DPCl the calculated values from the PEF agree reasonably well with the experimentally derived values for the bending and PCl stretching mode (to within 12 cm^{-1}). In view of the lack of observed higher vibrational bands of the HP (DP) stretching modes in the SVL emission spectra of HPCl (DPCl), the calculated harmonic HP and DP stretching frequencies obtained from the *ab initio* PEFs in the present study are probably more reliable than the corresponding experimentally derived harmonic values reported in Ref. 4.

For the $\tilde{A}\,^2A'$ state of HPCl and DPCl, the agreement between the fundamental vibrational frequencies of all three modes obtained from the PEF and the observed values from the LIF spectra of Ref. 4 is in general very good (to within 10 cm^{-1}; see Table V) It should be noted that for the $\tilde{A}\,^2A'$ state of DPCl, the $\tilde{A}(1,0,0)\leftarrow\tilde{X}(0,0,0)$ LIF band was too

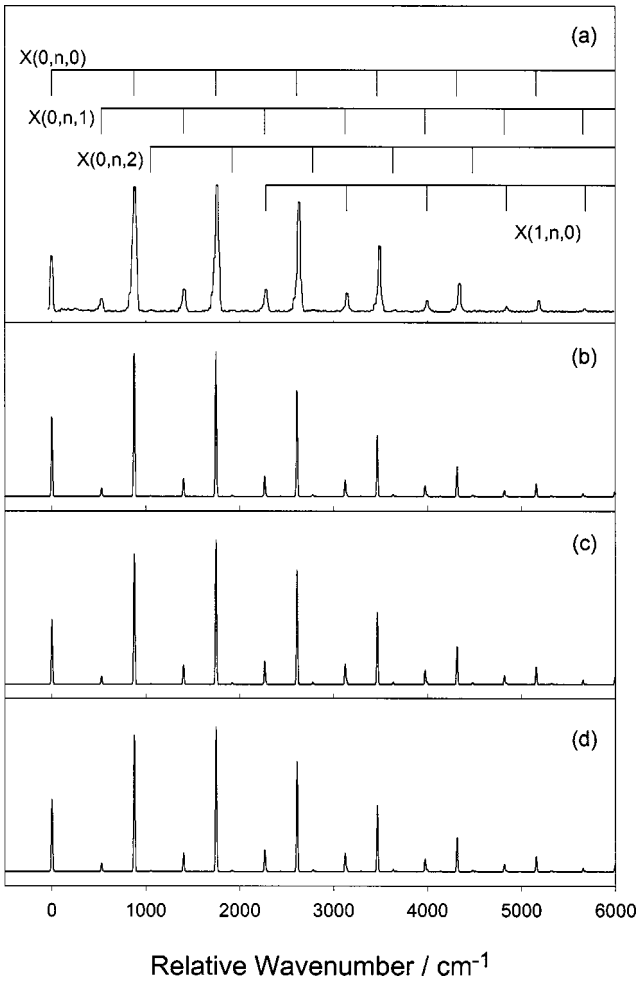

FIG. 1. The $\tilde{A}(0,0,0)\rightarrow\tilde{X}$ SVL emission spectrum of HPCl: (a) experimental spectrum from Ref. 4, (b) simulated spectrum employing the experimentally derived r_e^z geometry from Ref. 4 for both states (see Table III), (c) simulated spectrum employing the averaged *ab initio* geometry change upon deexcitation (see text), and (d) simulated spectrum employing the IFCA geometry of $r_e(\mathrm{PH})=1.406\,25$ Å, $\theta_e=116.08°$, and $r_e(\mathrm{PCl})=2.0035$ Å [averages of those used in simulating spectra (b) and (c); see text].

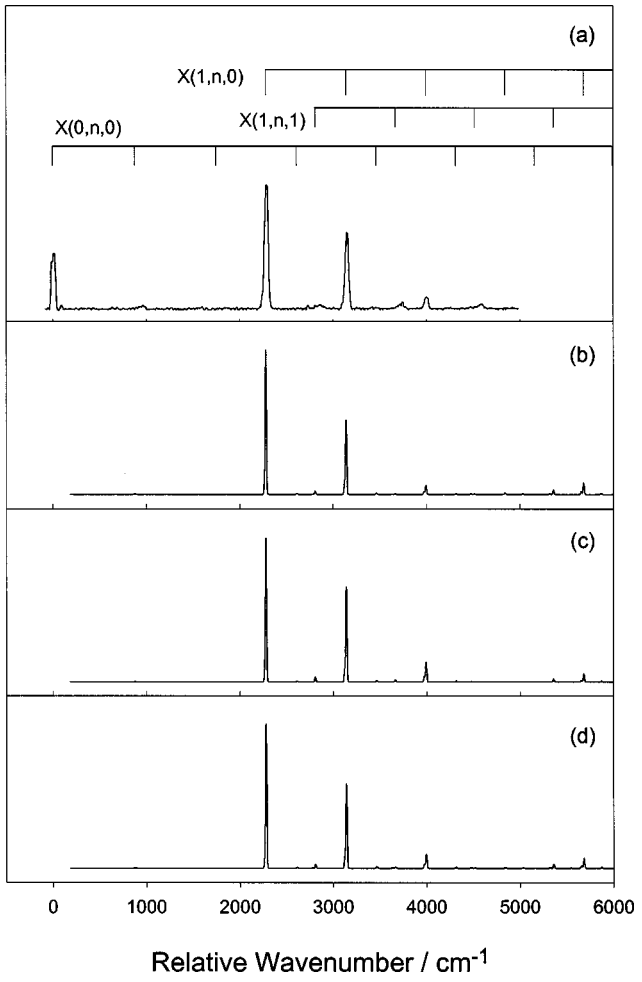

FIG. 2. The $\tilde{A}(1,1,0)\rightarrow\tilde{X}$ SVL emission spectum of HPCl: (a) experimental spectrum from Ref. 4, (b) simulated spectrum employing the experimentally derived r_e^z geometry from Ref. 4 for both states (see Table III), (c) simulated spectrum employing the averaged *ab initio* geometry change upon deexcitation (see text) and (d) simulated spectrum employing the IFCA geometry of $r_e(\mathrm{PH})=1.406\,25$ Å, $\theta_e=116.08°$, and $r_e(\mathrm{PCl})=2.0035$ Å [averages of those used in simulating spectra (b) and (c); see text].

weak to assign.[4] Regarding the harmonic vibrational frequencies of the $\tilde{A}\,^2A'$ state, Tackett *et al.*[4] were unable to find any bands involving $2\nu_1'$ in their LIP spectra of both HPCl and DPCl. Therefore, as with the $\tilde{X}\,^2A''$ state discussed above, the calculated harmonic frequencies of the HP and DP stretching modes of the $\tilde{A}\,^2A'$ state of HPCl and DPCl from the PEF are probably more reliable than the experimentally derived values reported in Ref. 4. For the bending and PCl stretching modes of the $\tilde{A}\,^2A'$ state of HPCl and DPCl, the agreement between the calculated harmonic vibrational frequencies and the observed values is within 28 cm^{-1}.

D. Calculated and observed transition energies, T_0 and T_e

The calculated transition energies obtained at different levels of theory are compared with the observed values in Table VI. Considering only the values from the relatively higher levels of calculation of the present study, the averaged T_e value of the $\tilde{A}\,^2A'-\tilde{X}\,^2A''$ transition of HPCl/DPCl is 2.743 eV (22 127.2 cm^{-1})$\pm$0.020 eV (170 cm^{-1}). The averaged calculated T_0 values, employing the harmonic vibrational frequencies obtained from the PEFs of the two electronic states reported here for zero-point vibrational energy corrections, is 2.731 eV (22 025.5 cm^{-1}) for HPCl, and 2.735 eV (22 061.7 cm^{-1}) for DPCl. The agreement between these averaged calculated T_0 values and the corresponding observed values from Ref. 4 is within 0.017 eV (135 cm^{-1}). No obvious trend can be identified in the calculated T_e values obtained at different levels of theory. It appears that the different contributions from basis set extension, core electrons, and relativity to the calculated relative electronic energy are probably not in the same direction, and hence would cancel each other at least to a certain extent. It is therefore concluded that any further improvements in the level of calculation would not change the computed relative electronic energy significantly, and a theoretical uncertainty of $\sim$0.02 eV (160 cm^{-1}) would be near the best achievable for *ab initio* relative electronic energies.

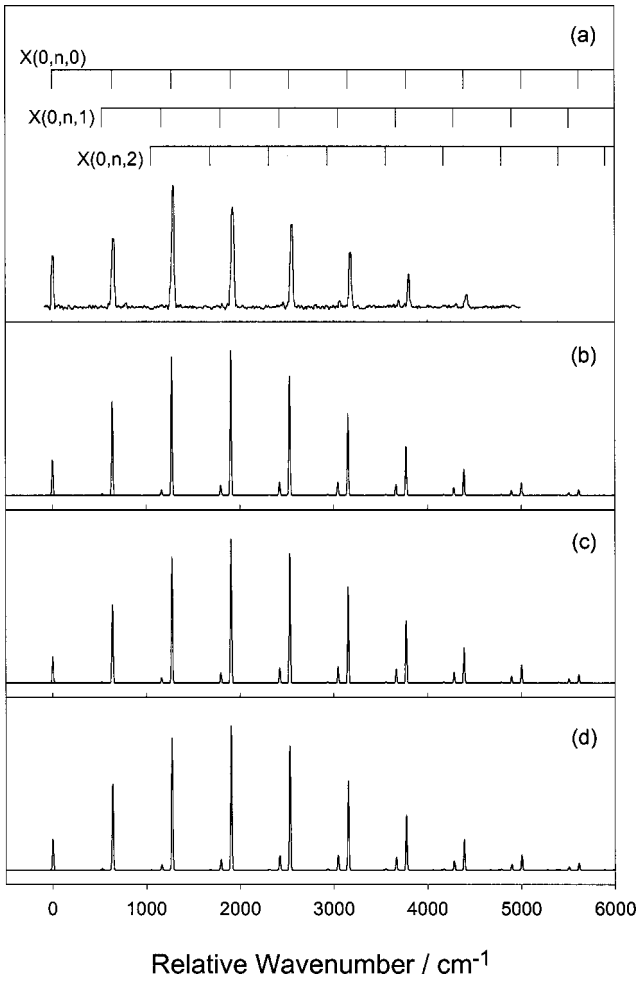

FIG. 3. The $\tilde{A}(0,0,0)\rightarrow\tilde{X}$ SVL emission spectum of DPCl: (a) experimental spectrum from Ref. 4, (b) simulated spectrum employing the experimentally derived r_e^z geometry from Ref. 4 for both states (see Table III), (c) simulated spectrum employing the averaged *ab initio* geometry change upon deexcitation and (d) simulated spectrum employing the IFCA geometry of $r_e(\mathrm{PH})=1.406\,25$ Å, $\theta_e=116.08°$, and $r_e(\mathrm{PCl})=2.0035$ Å [averages of those used in simulating spectra (b) and (c); see text].

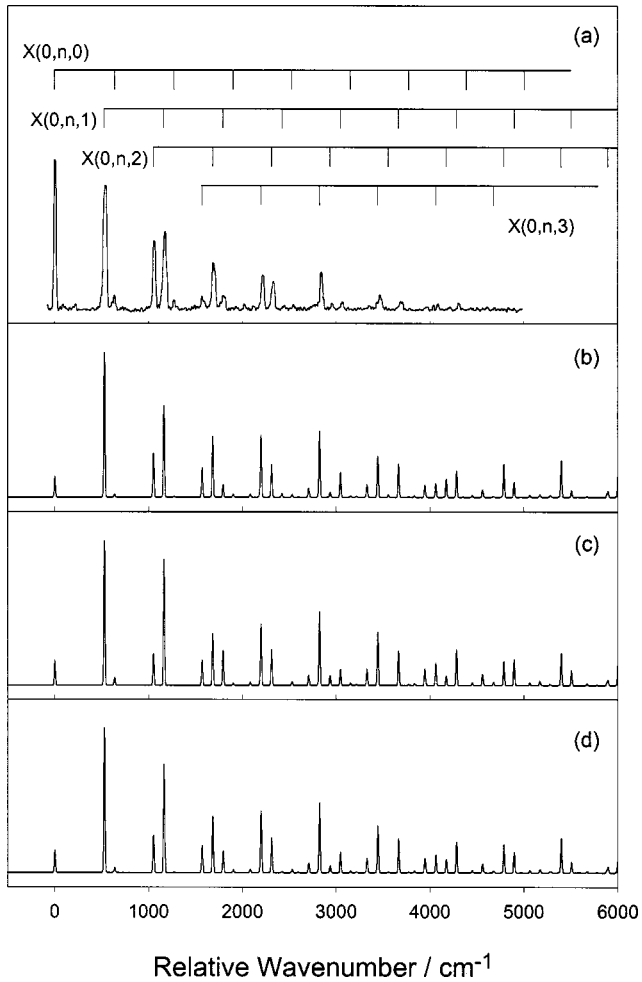

FIG. 4. The $\tilde{A}(0,1,2)\rightarrow\tilde{X}$ SVL emission spectum of DPCl: (a) experimental spectrum from Ref. 4, (b) simulated spectrum employing the experimentally derived r_e^z geometry from Ref. 4 for both states (see Table III), (c) simulated spectrum employing the averaged *ab initio* geometry change upon deexcitation, and (d) simulated spectrum employing the IFCA geometry of $r_e(\mathrm{PH})=1.406\,25$ Å, $\theta_e=116.08°$, and $r_e(\mathrm{PCl})=2.0035$ Å [averages of those used in simulating spectra (b) and (c); see text].

E. Comparison between simulated and observed SVL emission spectra of HPCl and DPCl

Figures 1–4 show the four observed SVL emission spectra published in Ref. 4 [top spectra (a) in Figs. 1–4]. Selected, corresponding simulated SVL emission spectra are also shown in Figs. 1–4 for comparison. These simulated spectra have been obtained employing the experimentally derived, estimated r_e^z geometrical parameters of the $\tilde{X}\,^2A''$ state from Ref. 4 [$r_e(\mathrm{HP})=2.0388$ Å, $r_e(\mathrm{PCl})=1.4158$ Å, and $\theta_e=95.02°$; see Table III] in all cases, and the following sets of geometrical parameters for the $\tilde{A}\,^2A'$ state for the different sets of simulated spectra [(b), (c), and (d)] shown in each figure. (b) The experimentally derived, estimated r_e^z bond lengths and angle from Ref. 4 were used for the $\tilde{A}\,^2A'$ state ($\theta_e=115.53°$ for the $\tilde{A}\,^2A'$ state; see Table III); (c) The averaged *ab initio* changes in the equilibrium bond lengths and angle upon deexcitation as discussed above were used together with the experimentally derived, estimated r_e^z geometrical parameters of the $\tilde{X}\,^2A''$ state to give the geometrical parameters of the $\tilde{A}\,^2A'$ state [$r_e(\mathrm{PCl})=2.0020$ Å, $\theta_e=116.63°$, and $r_e(\mathrm{HP})=1.4085$ Å]; (d) The IFCA bond lengths of $r_e(\mathrm{PCl})=2.0035$ and $r_e(\mathrm{HP})=1.4063$ Å and bond angle of $\theta_e=116.08°$ were used for the $\tilde{A}\,^2A'$ state [these are the averaged values between those used to obtain simulated spectra (b) and (c)].

In the comparison between the observed and simulated spectra, it should be borne in mind that the experimental spectra from Ref. 4 were not corrected for wavelength-dependent response of the monochromator and detection system. In addition, the variation of the electronic transition dipole moment over the electronic band has been ignored in the simulated spectra. In spite of these experimental and theoretical shortcomings, it can be seen from Figs. 1–4 that the overall agreement between the observed and simulated spectra is very good. All vibrational features of the observed SVL emission spectra are reasonably well produced in the corresponding simulated spectra shown. Before comparing the observed and simulated spectra in more detail, it should be noted that the changes in the bond lengths upon deexcitation

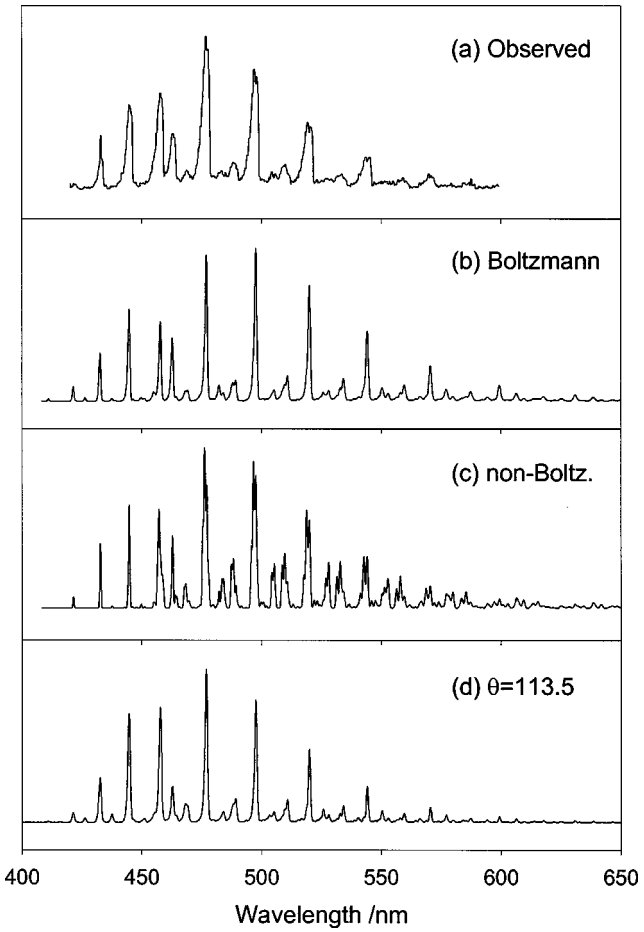

FIG. 5. The chemiluminescence spectrum of HPCl: (a) Experimental spectrum from Ref. 2, (b) simulated spectrum, employing the IFCA geometry of the $\tilde{A}\,^2A'$ state [see figure caption (d) of Figs. 1–4 and text], with a Boltzmann distribution for the populations of the low-lying vibrational levels of the $\tilde{A}\,^2A'$ state at a vibrational temperature of 800 K (c) simulated spectrum, employing the IFCA geometry of the $\tilde{A}\,^2A'$ state [see figure caption (d) of Figs. 1–4 and text], with a non-Boltzmann distribution for the populations of the low-lying vibrational levels of $\tilde{A}\,^2A'$ state (weights of different SVL emissions used to obtain the simulated spectrum are given in Table VII), and (d) simulated spectrum, employing an IFCA bond angle of 113.5°, with a Boltzmann distribution at 800 K (see text).

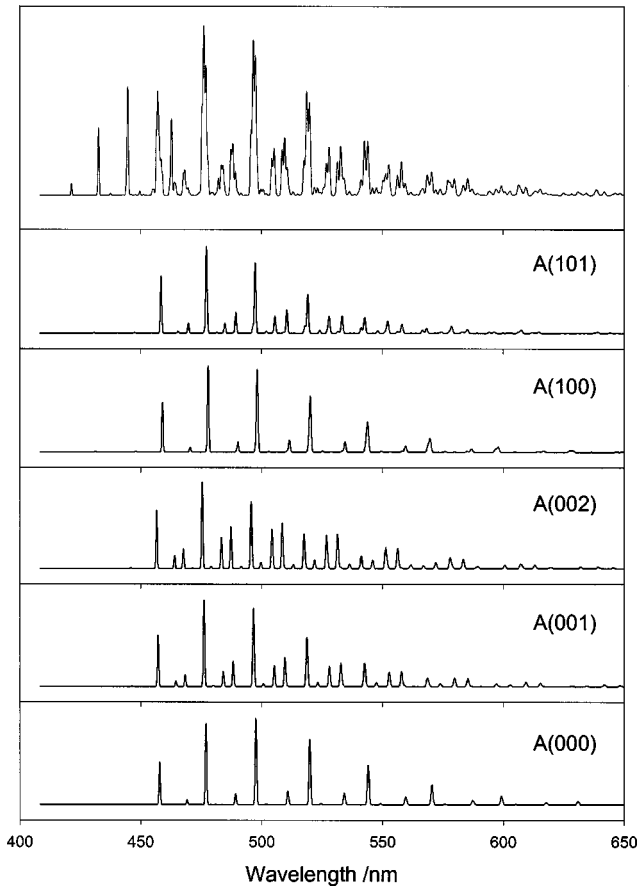

FIG. 6. Some simulated SVL emission spectra, which contribute to the simulated "composite" chemiluminescence spectrum [top trace same as Fig. 5(c); see text].

from the *ab initio* calculations and from the experimentally derived, estimated r_e^z structures are very similar, as discussed, and are also relatively small in magnitude. The major geometrical change upon deexcitation lies in the bond angle and the major observed vibrational structure involves mainly the bending mode. In addition, it has been noted above that the best averaged *ab initio* bond angle of the $\tilde{A}\,^2A'$ state differs from the experimentally derived, estimated r_e^z value of Ref. 4 by more than 1°. Hence, the major concern of the geometrical change upon deexcitation lies in the bond angle of the $\tilde{A}\,^2A'$ state. In view of the above considerations, the three sets of excited state geometrical parameters used for the simulated spectra (b), (c), and (d) shown in Figs. 1–4, may be viewed as representatives of the variation of the bond angle of the $\tilde{A}\,^2A'$ state used in the IFCA procedure. Bearing the above considerations in mind, the three sets of simulated spectra [(b), (c), and (d) in Figs. 1–4] are compared with the corresponding observed spectra [(a) in Figs. 1–4] as follows.

For the $\tilde{A}(0,0,0)$ SVL emission (Fig. 1), the simulated spectrum (b) appears to match best with the observed spectrum (a) among the three simulated spectra. However, for the $\tilde{A}(1,1,0)$ SVL emission (Fig. 2) with the simplest vibrational structure, the simulated spectrum (b) underestimates slightly the relative intensity of the $X(1,1,0)$ vibrational component, and the simulated spectrum (d) matches best with the observed spectrum (a). For the $\tilde{A}(0,1,2)$ SVL emission of DPCl (Fig. 4), all three simulated spectra (b), (c), and (d) give very long vibrational progressions with significant relative intensities even beyond the 5000 cm^{-1} region (the wave number scale is displacement from the laser excitation frequency, giving a direct measure of the ground state vibrational energy; see Ref. 4), while the relative intensities of the higher components of the vibrational structure of the lower electronic state in the observed spectrum (a) tail off at the ca. 4000 cm^{-1} region. These comparisons suggest that the efficiency of the detector system used in Ref. 4 to obtain the SVL $\tilde{A}(0,1,2)$ emission spectrum of DPCl is very likely decreasing towards lower emission energies (corresponding to emission to higher vibrational levels of the $\tilde{X}\,^2A''$ state). Bearing this in mind, it appears that the simulated spectrum (d), which is a compromise between the simulated spectra (b) and (c), matches best with the observed spectrum (a). Summing up, based on the comparisons between the simulated and observed spectra discussed above, it is concluded that

spectra (d) in Figs. 1, 2, and 4 have the best overall matches with the corresponding observed spectra (a), and the IFCA geometry of the $\tilde{A}\,^2A'$ state is $r_e(\mathrm{PCl}) = 2.0035 \pm 0.0015$ Å, $\theta_e = 116.08 \pm 0.60°$, and $r_e(\mathrm{HP}) = 1.4063 \pm 0.0015$ Å. It is noted that the IFCA bond angle of 116.08° obtained for the $\tilde{A}\,^2A'$ state is an average value between those used to obtain spectra (b) and (c) [115.53° (experimentally derived, estimated r_e^z value of Ref. 4) and 116.63° (based on the averaged *ab initio* geometry change obtained here) respectively], and spectral simulations reported here suggests that the true equilibrium bond angle of the $\tilde{A}\,^2A'$ state lies on the larger side of the uncertainty of the experimentally derived, estimated r_e^z value of Ref. 4, and on the smaller side of that of the best *ab initio* value obtained here. Since the observed SVL emission spectra are not corrected for wavelength dependency of the detector system, a rather large uncertainty of ±0.60° has been given to the IFCA bond angle. Nevertheless, the experimentally derived, estimated r_e^z values of Ref. 4 and the very consistent *ab initio* values obtained here (Table VI) are just within this uncertainty. However, the difference of ~3.6° between the present IFCA bond angle of 116.08°, which has been obtained including anharmonicity in the calculation of the FC factors, and the earlier IFCA value of 112.6° obtained within the harmonic oscillator model is quite large and clearly way beyond the uncertainty of ±0.60°. The considerably smaller, earlier IFCA value of Ref. 1 is obviously in error. This is at least partly due to the neglect of anharmonicity in our previous calculations of FC factors, but is also partly due to the assumption of a Boltzmann distribution of the population in the low-lying vibrational levels of the upper electronic state used in the simulation of the overlapping vibrational bands in the chemiluminescence spectrum. We will come back to this, when the chemiluminescence spectrum is considered.

Regarding the $\tilde{A}(0,0,0)$ SVL emission spectrum of DPCl, although the overall match between the simulated and observed spectra is reasonably good for all three simulated spectra shown in Fig. 3, simulated spectra obtained in the IFCA procedure cannot reproduce the rather strong relative intensity of the $\tilde{X}(0,2,0)$ vibrational component observed at an energy of 1277.3 cm^{-1} from the ground vibrational level of the lower electronic state. All simulated spectra (b), (c), and (d) give a gradual and smooth change in the relative intensities of successive vibrational components in the main bending progression. However, the $\tilde{X}(0,2,0)$ component in the observed spectrum [Fig. 3(a)] appears to have a relative intensity, which is significantly stronger than that expected from the trend of the rest in the vibrational progression. A simulated SVL $\tilde{A}(0,0,0)$ emission spectrum of DPCl, which gives the $\tilde{X}(0,2,0)$ component of maximum relative intensity in the vibrational progression, requires an excited state bond angle significantly smaller than 115.0° and such a spectrum still gives a gradual and smooth change in the relative intensities of all members of the $\tilde{X}(0,n,0)$ series. We are unable to explain this abnormality in the relative intensity of the $\tilde{X}(0,2,0)$ component in the observed SVL $\tilde{A}(0,0,0)$ spectrum of DPCl based on our spectral simulation, and hence have not considered this emission in deriving the IFCA geometry of the $\tilde{A}$ state.

From computed FC factors, the $\tilde{X}(1,n,0)$ series has a nontrivial contribution to the SVL $\tilde{A}(0,0,0)$ emission spectrum of HPCl [see the bar diagrams and the vibrational designations shown in Fig. 1(a)]. Vibrational components of the $\tilde{X}(1,n,0)$ series are energetically close to, and hence overlap with, vibrational components of the $\tilde{X}(0,n+2,1)$ series [for example, the $\tilde{X}(1,0,0)$ and $\tilde{X}(0,2,1)$ vibrational levels were calculated to be only 12.6 cm^{-1} apart; see Table II]. For the SVL $\tilde{A}(1,1,0)$ emission of HPCl, computed FC factors suggest that the very weak feature is due to the $\tilde{X}(1,n,1)$ and $\tilde{X}(0,n,0)$ series [see Fig. 2(a)]. Similarly, the very weak feature in the SVL $\tilde{A}(0,0,0)$ emission spectrum of DPCl is due to the $\tilde{X}(0,n,1)$, and to a smaller extent $\tilde{X}(0,n,2)$, series. However, the $\tilde{X}(1,0,1)$ and $\tilde{X}(1,0,2)$ components of DPCl given in Table II of Ref. 4 do not have significant computed FC factors according to our calculations on the SVL $\tilde{A}(0,0,0)$ and (0,1,2) emissions of DPCl and we are unable to assign these vibrational components in our simulated spectra in Figs. 3 and 4. Perhaps these vibrational components were observed in unpublished dispersed fluorescence spectra of DPCl, which are not available to us.

TABLE VII. The relative weights used in the non-Boltzmann distribution of the populations of some low-lying vibrational levels of the $\tilde{A}\,^2A'$ state of HPCl employed in simulating the chemiluminescence spectrum as shown in Fig. 5(c) and Fig. 6 (top trace); see text.

$\tilde{A}(\nu_1', \nu_2', \nu_2')$	Weights[a] (present work)	Weights (Ref. 3)
(0,0,0)	0.15	0.65
(0,0,1)	0.34	
(0,1,0)	0.10	0.20
(0,0,2)	0.21	
(0,1,1)	0.02	
(0,2,0)	0.04	0.10
(0,3,0)	0.01	0.05
(1,0,0)	0.05	
(1,0,1)	0.09	

[a]Normalized to unity.

F. Comparison between simulated and observed chemiluminescence spectra of HPCl

Figure 5 compares the observed chemiluminescence spectrum of HPCl reported in Ref. 2 [Fig. 5(a)] with the corresponding simulated spectra obtained in the present study. The simulated emission spectrum Fig. 5(c), includes contributions from a non-Boltzmann distribution of the low-lying vibrational levels of the $\tilde{A}\,^2A'$ state, with the relative weights of the different emissions involved given in Table VII. The simulated emission spectrum Fig. 5(b), has employed a Boltzmann distribution with a vibrational temperature of 800 K. This simulated spectrum is the best match with the observed spectrum obtainable based on a Boltzmann distribution (the only variable in the match is the vibrational temperature). Both simulated spectra Figs. 5(b) and 5(c), have employed the IFCA geometry for the $\tilde{A}\,^2A'$ state of HPCl, obtained above, when the SVL emissions were con-

sidered. Figure 5(d) shows the simulated spectrum including contributions from bands based on a Boltzmann upper state distribution with a temperature of 800 K, but with an IFCA bond angle of 113.5° (and the r_e's from the PEF) for the $\tilde{A}\,^2A'$ state of HPCl. Figure 6 shows simulated spectra of most of the individual SVL emissions, which have significant contributions to the simulated composite spectrum [top trace in Fig. 6, which is the same as Fig. 5(c)].

Before each simulated and observed chemiluminescence spectrum of HPCl are compared in detail, it should be noted that the relative intensities of the different members of the main vibrational progression observed in the chemiluminescence spectrum[2] of HPCl, the $\tilde{A}(0,0,0)\rightarrow\tilde{X}(0,n,0)$ progression [Fig. 5(a)], do not match exactly with those observed in the SVL $\tilde{A}(0,0,0)$ emission spectrum of Ref. 4 [see vibrational assignments given in Fig. 1(a)]. Specifically, the relative intensities of the higher members of this vibrational series in the chemiluminescence spectrum decrease faster than those in the SVL emission spectrum, and the $\tilde{X}(0,2,0)$ component in the SVL $\tilde{A}(0,0,0)$ emission spectrum has the maximum relative intensity, while in the observed chemiluminescence spectrum, the $\tilde{X}(0,1,0)$ component is the strongest. Just considering the experimental chemiluminescence spectrum of Ref. 2 [Fig. 5(a)] and the SVL $\tilde{A}(0,0,0)$ emission spectrum of Ref. 4 [Fig. 1(a)], it is unclear whether the discrepancies between the two observed spectra in the main $\tilde{A}(0,0,0)\rightarrow\tilde{X}(0,n,0)$ progression is due to the different wavelength dependences of the detector systems used in the two different experimental setups (the chemiluminescence spectrum was not corrected for any wavelength-dependent instrumental response[18]) or due to overlapping emissions arising from low-lying excited vibrational levels of the upper state in the chemiluminescence spectrum[2] [the SVL $\tilde{A}(0,0,0)$ emission[4] is obviously free from such overlapping bands]. Since the wavelength dependences of the detector systems used in Refs. 2 and 4 are unavailable to us, we can only ignore them in the following discussion and assume that the discrepancies between the reported SVL $\tilde{A}(0,0,0)$ emission spectrum and the chemiluminescence spectrum are merely due to extra bands in the latter arising from emissions from higher vibrational levels of the upper electronic state.

First, the simulated spectrum with a bond angle of 113.5° for the $\tilde{A}\,^2A'$ state [Fig. 5(d)] is considered. The main features of this simulated spectrum match almost exactly with those of the observed spectrum [Fig. 5(a)], except for the ''shoulders'' or ''multiplet'' structure associated with the observed main $\tilde{X}(0,n,0)$ series and, to a lesser extent, small discrepancies in the region of ca. 450 nm. The bond angle of the $\tilde{A}\,^2A'$ state employed in this simulated spectrum (including anharmonicity) is larger than the IFCA value obtained previously with the harmonic oscillator model,[1] but is still smaller than the very consistent *ab initio* values by ca. 3°. Based on our previous conclusion that excessive variations of geometrical parameters (from reliable *ab initio* values) in the IFCA procedure are not recommended,[10] and also noting the good agreement between the simulated and observed SVL mission spectra using the IFCA bond angle of 116.08° for the $\tilde{A}\,^2A'$ state discussed above, we have to conclude that such a good match between the simulated and observed spectra of Figs. 5(d) and 5(a), respectively, is fortuitous. This is similar to the near exact match between the simulated spectrum obtained within the harmonic oscillator model and the observed spectrum reported previously in Ref. 1, employing an IFCA bond angle of 112.6° for the $\tilde{A}\,^2A'$ state. With the SVL emission spectra of Ref. 4 available at present, and the spectral simulation including anharmonicity and the systematic high-level *ab initio* geometry optimization calculations carried out in the present study, the bond angle of the $\tilde{A}\,^2A'$ state of HPCl has now been established to be $116.08\pm0.60°$ as discussed above. As a result, in the simulation of the chemiluminescence spectrum reported in Ref. 2, only the populations of the low-lying excited vibrational levels of the $\tilde{A}\,^2A'$ state need to be considered, as follows.

Employing the JFCA geometry of the $\tilde{A}\,^2A'$ state of HPCl obtained in the present investigation and assuming a Boltzmann distribution for the vibrational populations of the upper state in the simulation, the best match obtained between the simulated and observed spectrum [Figs. 5(b) and 5(a), respectively] is with a vibrational temperature of 800 K. Although the overall observed vibrational envelope is produced in the simulated spectrum, the match between Figs. 5(a) and 5(b) is not exact. Specifically, the discrepancies in the main $\tilde{X}(0,n,0)$ series are similar to those between the observed SVL $\tilde{A}(0,0,0)$ emission [Fig. 1(a)] and the observed chemiluminescence spectrum [Fig. 5(a)] discussed above. In addition, the match between the simulated and observed chemiluminescence spectra in the region arising from higher vibrational levels in the $\tilde{A}\,^2A'$ state (ca. 450 nm) is also not exact. It was found that it was not possible to improve the match further by adjusting only the vibrational temperature used in the Boltzmann distribution. Consequently, a non-Boltzmann distribution involving higher vibrational levels of the upper state has to be considered, as proposed in Ref. 3.

With a non-Boltzmann distribution of relative weights of populations in various vibrational levels of the $\tilde{A}\,^2A'$ state of HPCl given in Table VII, the simulated spectrum shown in Fig. 5(c) gives a better match with the observed spectrum [Fig. 5(a)] in the main $\tilde{X}(0,n,0)$ series than that obtained with a Boltzmann distribution [Fig. 5(b)], and also gives multiplet structures in the vibrational components in the higher wavelength region. It should be noted that the multiplet structure in each vibrational component of the observed spectrum is not well resolved, and also with a non-Boltzmann distribution, the choices of relative weights of vibrational populations and the low-lying vibrational levels of the upper state from which emissions are included in the spectral simulation, which give the best match, may not be unique. In view of these experimental and theoretical limitations, the main aim in obtaining the simulated spectrum shown in Fig. 5(c) has been to match the overall pattern of the observed vibrational structure with the smallest numbers of SVL emissions from the low-lying vibrational levels of the upper state. Although the match between Figs. 5(a) and 5(c) is not exact, we believe that this aim has been largely achieved. It should be pointed out that, it is contributions

from the SVL $\tilde{A}(1,0,1)$, (0,0,2), and (0,0,1) emissions, which have shifted the strongest vibrational component in the simulated chemiluminescence spectrum (top trace in Fig. 6) from the strongest $\tilde{X}(0,2,0)$ component of the $\tilde{A}(0,0,0) \rightarrow \tilde{X}(0,n,0)$ series (bottom trace in Fig. 6) to the $\tilde{X}(0,1,0)$ component [see Fig. 1(a) for their assignments/positions], and lead to good agreement between simulation and observation in the pattern of the main vibrational structure in the 450–550 nm region of the chemiluminescence spectrum. SVL emissions from higher vibrational levels in the $\tilde{A}\,^2A'$ state than those shown in Table VII have been considered, but their inclusion did not improve the match between the simulated and observed spectra. One main difficulty in the match is the balance between the agreement for the main $\tilde{X}(0,n,0)$ series and the agreement for the other weaker series. Nevertheless, the region of near 450 nm is dominated by the $\tilde{A}(0,n,0) \rightarrow \tilde{X}$ emissions, with $n=1-3$, which have only weak contributions to the higher wavelength region, and hence their individual SVL emissions are not shown in Fig. 6. Summing up, spectral simulation carried out in the present study confirms that the chemiluminescence spectrum reported in Ref. 2 has a non-Boltzmann distribution in the upper state, which should be close to the relative populations given in Table VII.

IV. CONCLUDING REMARKS

Near state-of-the-art level *ab initio* calculations have been carried out on the $\tilde{A}\,^2A'$ and $\tilde{X}\,^2A''$ states of HPCl, giving highly consistent and reliable computed equilibrium geometrical parameters, PEFs, fundamental and harmonic vibrational frequencies of, and transition energies between, the two states. Simulated SVL emission spectra of HPCl and DPCl and chemiluminescence spectrum of HPCl have been obtained based on computed FC factors which consider anharmonicity explicitly. Experimentally derived equilibrium geometrical parameters for the $\tilde{A}\,^2A'$ state of HPCl have been obtained via the IFCA procedure based on comparison between simulated and observed SVL emission spectra. These IFCA geometrical parameters of the $\tilde{A}\,^2A'$ state obtained in the present investigation, based on simulated spectra including anharmonicity, agree much better with the state-of-the-art *ab initio* values than those reported previously based on simulated spectra obtained within the harmonic oscillator model,[1] particularly for the bond angle. In addition, the IFCA bond angle obtained here has a value which is in between highly consistent *ab initio* values and the experimentally derived, estimated r_e^z value reported in Ref. 4. An uncertainty of $\pm 0.60°$, which covers highly consistent *ab initio* values and the experimentally derived, estimated r_e^z value of Ref. 4, is quoted here.

Simulated chemiluminescence spectra reported here, which include anharmonicity in each electronic state, suggest a non-Boltzmann distribution of vibrational populations in the upper electronic state, confirming the proposal of Baraille *et al.*[3] However, we are unable to compare the full set of relative weights of the vibrational populations in the $\tilde{A}\,^2A'$ state used here to produce Fig. 5(c) with that used to produce the simulated spectrum of Ref. 3 [Fig. 2(b) therein], as Baraille *et al.* has only reported the partition function coefficients of the $\tilde{A}(0,n,0)$ levels for $n=0$ to 3 (0.65, 0.20, 0.10, and 0.05, respectively; see Table VII) used in their spectral simulation, despite the involvement of the SVL $\tilde{A}(0,0,p) \rightarrow \tilde{X}$ emissions in their simulation. Our simulations do agree with their simulations in that some SVL $\tilde{A}(0,0,p)$ emissions are involved in the chemiluminescence spectrum as discussed above (see also Table VII). However, the relative vibrational populations of the $\tilde{A}(0,n,0)$ levels for $n=0-3$ obtained here only agree qualitatively with their values. At the same time, we find that including SVL $\tilde{A}(1,0,p)$ emissions with $p=0$ and 1 helps to improve the match between the simulated and observed spectra, but based on their computed FC factors, Baraille *et al.* concluded otherwise. Since HPCl was produced in the exothermic reaction between PCl, and H atom,[2] it is not unreasonable to expect HPCl to be produced vibrationally excited in the HP stretching mode, as HP is the newly formed bond. Considering the simulated spectrum of HPCl in Ref. 3, it appears that its overall pattern of vibrational structure is similar to that of the SVL $\tilde{A}(0,0,0)$ emission of Ref. 4 [Fig. 1(a)], with the strongest simulated vibrational component at ca. 500 nm $[\tilde{X}(0,2,0)]$ in contrast to the strongest observed vibrational component at ca. 450 nm $[\tilde{X}(0,1,0)]$ in the chemiluminescence spectrum of Ref. 2 (see Fig. 6). We can only conclude that our simulated spectrum in Fig. 5(c) has a better match with the observed chemiluminescence spectrum[2] than the simulated spectrum reported in Ref. 3.

In the comparison between simulated and observed spectra, one major source of uncertainty comes from the wavelength dependence of the detector system used to obtain the experimental spectrum, which is usually not corrected in published observed spectra. On the theoretical side, the variation of transition moment over a spectral band needs to be considered in order to give more reliable simulated spectra. Incorporating this into our on-going research program of spectral simulation is underway.

ACKNOWLEDGMENTS

The authors are grateful to the Research Grant Council (RGC) of the Hong Kong Special Administrative Region (HKSAR, Grant Nos. AoE/B-10/1 and PolyU 5003/03P) and the Research Committee of the Hong Kong Polytechnic University, HKSAR (Grant No. G-T635) for financial support. The EPSRC (UK) National Service for Computational Chemistry Software is acknowledged for providing computational resources in carrying out the *ab initio* calculations of this study. This work was also supported by the Leverhulme Trust, and helpful discussions with Dr. Chris Whitehead (Manchester, UK) are acknowledged.

[1] E. P. F. Lee, D. K. W. Mok, J. M. Dyke, and F.-T. Chau, Chem. Phys. Lett. **340**, 349 (2001).
[2] M. J. Bramwell, D. M. Rogers, J. J. W. McDouall, and J. C. Whitehead, Chem. Phys. Lett. **331**, 483 (2000).
[3] I. Baraille, C. Larrieu, A. Dargelos, and M. Chaillet, Chem. Phys. **289**, 263 (2003).

[4] B. S. Tackett, S.-G. He, C. J. Evans, D. J. Clouthier, and R. H. Judge, J. Chem. Phys. **119**, 2037 (2003).
[5] C. Hampel, K. Peterson, and H.-J. Werner, Chem. Phys. Lett. **190**, 1 (1992).
[6] J. D. Watts, J. Gauss, and R. J. Bartlett, J. Chem. Phys. **98**, 8718 (1993).
[7] D. E. Woon and T. H. Dunning, Jr., J. Chem. Phys. **98**, 1358 (1993).
[8] S. Carter and N. C. Handy, J. Chem. Phys. **87**, 4294 (1987).
[9] F.-T. Chau, J. M. Dyke, E. P. F. Lee, and D. K. W. Mok, J. Chem. Phys. **115**, 5816 (2001).
[10] F. T. Chau, J. M. Dyke, E. P. F. Lee, and D. K. W. Mok, J. Chem. Phys. **118**, 4025 (2003).
[11] J. K. G. Watson, Mol. Phys. **15**, 479 (1968).
[12] J. K. G. Watson, Mol. Phys. **19**, 465 (1970).
[13] T. H. Dunning, Jr., K. A. Peterson, and A. K. Wilson, J. Chem. Phys. **114**, 9244 (2001).
[14] D. Feller, K. A. Peterson, W. A. de Jong, and D. A. Dixon, J. Chem. Phys. **118**, 3510 (2003).
[15] K. A. Peterson and T. H. Dunning, J. Chem. Phys. **117**, 10548 (2002).
[16] X. Cao and M. Dolg, J. Chem. Phys. **115**, 7348 (2001); Hermann Stoll (stoll@theochem.uni-stuttgart.de) or Michael Dolg (dolg@thch.uni-bonn.de or m.dolg@uni-koeln.de)
[17] MOLPRO is a package of *ab initio* programs written by H.-J. Werner and P. J. Knowles with contributions from J. Almlöf, R. D. Amos, A. Berning *et al.*
[18] C. Whitehead (private communication).